The Focusing of Electron Flow and a Veselago Lens in Graphene p-n Junctions
Vadim V. Cheianov, *et al.*
Science **315**, 1252 (2007);
DOI: 10.1126/science.1138020

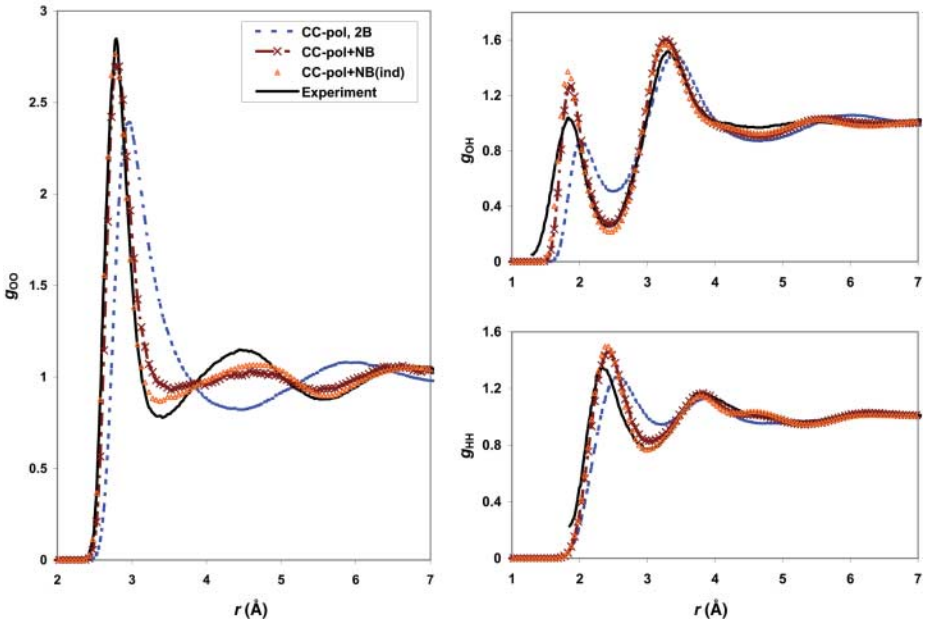

Fig. 3. Atom-atom radial distribution functions from MD simulations based on the CC-pol potential. See text for explanations of acronyms. The experimental curves are from (*30*).

could extrapolate this dependence to obtain 3.8 hydrogen bonds for the CC-pol+NB model. Thus, this model supports the standard picture of water, wherein each molecule is on average almost tetrahedrally coordinated, rather than the lower coordination geometry proposed in (*3*, *5*). With the use of only the CC-pol pair potential, the simulations gave a very large coordination number, 11.9 (the extrapolated number of hydrogen bonds equal to 2.7). Hence, the many-body interactions play an important role in determining the structure of liquid water, particularly in predicting tetrahedral coordination.

The ab initio water pair potential developed in this work recovers well a diverse range of experimental data from water dimer to liquid water. It predicts dimer spectra and second virial coefficients that not only agree well with existing experimental data, but also can be considered to complement experiments in spectral or temperature ranges inaccessible to measurement. When the CC-pol potential together with an earlier representation of three-body forces (*18*, *19*) was used in simulations of liquid water, the predictions agreed well with the neutron and x-ray diffraction data. These predictions, made entirely from first principles, are of comparable accuracy to results of simulations with empirical potentials fitted to liquid water experimental data.

We believe that the ab initio force field presented here will find numerous applications in predicting the properties of water. It can be used, for example, to resolve the current controversies about the coordination of water molecules in the liquid (*3*–*6*). The analysis of the temporal structures in MD simulations should provide the ultimate picture of liquid water. The force field can also be used to investigate the numerous polymorphic forms of ice. Important applications can be made in extreme regimes where empirical potentials fail completely, such as supercritical, overcooled, or confined water.

Further improvements in the first-principles predictions for water should take account of the monomer flexibility and of quantum effects in the liquid simulations. For the former case, the first step has recently been attained (*23*). Quantum effects in molecular simulations can be accounted for by either path-integral MC or centroid MD (*25*) methods.

References and Notes

1. K. Liu, J. Cruzan, R. Saykally, *Science* **271**, 929 (1996).
2. J. K. Gregory, D. C. Clary, K. Liu, M. G. Brown, R. Saykally, *Science* **275**, 814 (1997).
3. Ph. Wernet *et al.*, *Science* **304**, 995 (2004); published online 1 April 2004 (10.1126/science.1096205).
4. J. D. Smith *et al.*, *Science* **306**, 851 (2004).
5. A. Nilsson *et al.*, *Science* **308**, 793a (2005).
6. J. D. Smith *et al.*, *Science* **308**, 793b (2005).
7. D. Laage, J. T. Hynes, *Science* **311**, 832 (2006); published online 25 January 2006 (10.1126/science.1122154).
8. J. VandeVondele *et al.*, *J. Chem. Phys.* **122**, 014515 (2005).
9. M. Sharma, Y. Wu, R. Car, *Int. J. Quantum Chem.* **95**, 821 (2003).
10. M. Allesch, E. Schwegler, F. Gygi, G. Galli, *J. Chem. Phys.* **120**, 5192 (2004).
11. C. Millot, A. J. Stone, *Mol. Phys.* **77**, 439 (1992).
12. E. M. Mas *et al.*, *J. Chem. Phys.* **113**, 6687 (2000).
13. C. J. Burnham, S. S. Xantheas, *J. Chem. Phys.* **116**, 1500 (2002).
14. C. J. Burnham, S. S. Xantheas, *J. Chem. Phys.* **116**, 5115 (2002).
15. G. S. Fanourgakis, S. S. Xantheas, *J. Phys. Chem. A* **110**, 4100 (2006).
16. R. Bukowski, K. Szalewicz, G. C. Groenenboom, A. van der Avoird, *J. Chem. Phys.* **125**, 044301 (2006).
17. G. S. Tschumper *et al.*, *J. Chem. Phys.* **116**, 690 (2002).
18. E. M. Mas, R. Bukowski, K. Szalewicz, *J. Chem. Phys.* **118**, 4386 (2003).
19. E. M. Mas, R. Bukowski, K. Szalewicz, *J. Chem. Phys.* **118**, 4404 (2003).
20. R. S. Fellers, C. Leforestier, L. B. Braly, M. G. Brown, R. J. Saykally, *Science* **284**, 945 (1999).
21. G. C. Groenenboom *et al.*, *J. Chem. Phys.* **113**, 6702 (2000).
22. R. S. Fellers, L. B. Braly, R. J. Saykally, C. Leforestier, *J. Chem. Phys.* **110**, 6306 (1999).
23. K. Szalewicz, G. Murdachaew, R. Bukowski, O. Akin-Ojo, C. Leforestier, in *Lecture Series on Computer and Computational Science: ICCMSE 2006*, G. Maroulis, T. Simos, Eds. (Brill Academic, Leiden, Netherlands, 2006), vol. 6, pp. 482–491.
24. A. H. Harvey, E. W. Lemmon, *J. Phys. Chem. Ref. Data* **33**, 369 (2004).
25. L. Hernández de la Peña, P. G. Kusalik, *J. Chem. Phys.* **121**, 5992 (2004).
26. W. L. Jorgensen, J. Chandrasekhar, J. D. Madura, R. W. Impey, M. L. Klein, *J. Chem. Phys.* **79**, 926 (1983).
27. N. Goldman, C. Leforestier, R. J. Saykally, *Philos. Trans. R. Soc. London Ser. A* **363**, 493 (2005).
28. W. L. Jorgensen, *J. Chem. Phys.* **77**, 4156 (1982).
29. R. Mills, *J. Phys. Chem.* **77**, 685 (1973).
30. A. K. Soper, *Chem. Phys.* **258**, 121 (2000).
31. F. N. Keutsch, N. Goldman, H. A. Harker, C. Leforestier, R. J. Saykally, *Mol. Phys.* **101**, 3477 (2003).
32. F. N. Keutsch *et al.*, *J. Chem. Phys.* **119**, 8927 (2003).
33. S. Kuwajima, A. Warshel, *J. Phys. Chem.* **94**, 460 (1990).
34. N. Goldman *et al.*, *J. Chem. Phys.* **116**, 10148 (2002).
35. C. Leforestier, F. Gatti, R. Fellers, R. Saykally, *J. Chem. Phys.* **117**, 8710 (2002).

36. We thank C. Leforestier for many discussions of the water dimer spectra. Supported by NSF grants CHE-0239611 and CHE-0555979.

16 October 2006; accepted 26 January 2007
10.1126/science.1136371

The Focusing of Electron Flow and a Veselago Lens in Graphene *p-n* Junctions

Vadim V. Cheianov,[1]* Vladimir Fal'ko,[1] B. L. Altshuler[2,3]

The focusing of electric current by a single *p-n* junction in graphene is theoretically predicted. Precise focusing may be achieved by fine-tuning the densities of carriers on the *n*- and *p*-sides of the junction to equal values. This finding may be useful for the engineering of electronic lenses and focused beam splitters using gate-controlled *n-p-n* junctions in graphene-based transistors.

There are many similarities between optics and electronics. Rays in geometrical optics are analogous to classical trajectories of electrons, whereas electron de Broglie waves can interfere. The electron microscope is one example of the technological implementation of this similarity. The analogy with optics may also hold considerable potential for semiconductor elec-

tronics. In optics, transparent interfaces between materials are used in lenses and prisms to manipulate light beams. So far, interfaces have played a rather different role in semiconductors, where the central place was, for a long time, occupied by the *p-n* junction (PNJ). As a result of a depletion region near the contact between two semiconductors with different types of charge carriers (and a large energy gap), conventional PNJs are not suitable for precision manipulation of electron beams, which, if realized, may lead to a new functionality in microelectronics. From this perspective, a lot of promise is offered by the recently discovered (*1*) two-dimensional (2D) gapless semiconductor, graphene (*2*). Fine-tuning of the carrier density in graphene by means of electrical gates (*3*–*5*) or doping of the underlying substrate (*6*) was demonstrated, thus paving the way toward controllable ballistic PNJs. On the one hand, the PNJ in graphene is highly transparent for the charge carriers (*7*, *8*). On the other, the transmission of electrons through the *p-n* interface may resemble optical refraction (*9*) at the surface of metamaterials with negative refractive index (*10*–*12*): The straight interface is able to focus electric current, whereas a ballistic stripe of *p*-type graphene separating two *n*-type regions acts as a lens.

A feature of the band structure of graphene [monolayer of graphite (*2*, *13*)] is that its valence band (π) and conduction band (π*) touch each other. In the absence of doping, the Fermi level in graphene is at the energy that belongs to both bands and corresponds to the Bloch states in the corners of the hexagonal Brillouin zone of this 2D honeycomb crystal. For the states with a small quasi-momentum $\hbar\mathbf{k}$ counted from the corresponding corner of the Brillouin zone, the dispersion $\varepsilon(\mathbf{k})$ and group velocity $\mathbf{V} = d\varepsilon/d(\hbar\mathbf{k})$ of electrons are given by $\varepsilon_c(\mathbf{k}) = \hbar v k$, $\mathbf{V}_c = v\mathbf{k}/k$ in conduction band and $\varepsilon_v(\mathbf{k}) = -\hbar v k$, $\mathbf{V}_v = -v\mathbf{k}/k$ in valence band ($\hbar$ is Planck's constant, $h/2\pi$). Figure 1 illustrates such a dispersion for electrons in *n*-type graphene (on the left) and *p*-type graphene (on the right). In a split-gate structure (Fig. 1), voltages $\pm U$ applied to the two gates shift the degeneracy point of the electron dispersion cones down by $\hbar v k_c$ on the left and up by $\hbar v k_v$ on the right, thus forming a PNJ separating the *n*-region with the density of electrons $\rho_e = k_c^2/\pi$ and the *p*-region with the density of holes $\rho_h = k_v^2/\pi$. Here, $k_{c(v)}$ is the radius of the Fermi circle in the conduction (valence) band.

The transmission of charge through the PNJ bears resemblance to the refraction of light by left-handed metamaterials (*10*–*12*) with refractive index equal to −1. As a wave enters such a material, the relative direction of its group velocity **V** and the wave vector **k** of the wave reverses from parallel (in vacuum) to antiparallel. Therefore, upon refraction, the sign of the tangential velocity component of the propagating wave inverts, and the normal component remains the same. As a result, rays that diverge in vacuum become convergent after entering the metamaterial (*9*). For electrons in the PNJ, the Fermi momentum $k_{c(v)}$ plays the same role as the refractive index in geometrical optics, with the sign determined by the type of band—positive for the conduction band and negative for the valence band.

Indeed, let us consider, in Figs. 2A and 3A, a de Broglie wave of an electron approaching the PNJ from the *n*-side with the velocity $\mathbf{V} = (v\cos\theta_c, v\sin\theta_c)$ and the wave vector $\mathbf{k} = (k_c\cos\theta_c, k_c\sin\theta_c)$. At the interface, this wave is partly reflected to the state with the wave vector $\mathbf{k}' = (-k_c\cos\theta_c, k_c\sin\theta_c)$ and partly transmitted to the valence band state with the velocity $\mathbf{V} = (v\cos\theta_v, v\sin\theta_v)$ and the wave vector $\mathbf{k} = (-k_v\cos\theta_v, -k_v\sin\theta_v)$ on the *p*-side. For a sharp PNJ, the probability of the transmission is $\cos^2\theta_c/\cos^2(\tfrac{1}{2}\theta_c + \tfrac{1}{2}\theta_v)$ (*7*, *8*). Because the component of the electron momentum along a straight interface should be conserved, $k_c\sin\theta_c = -k_v\sin\theta_v$, which determines Snell's law for transmitted electrons.

$$\frac{\sin\theta_c}{\sin\theta_v} = -\frac{k_v}{k_c} \equiv n \qquad (1)$$

The negative sign of *n* in Eq. 1 implies that the PNJ transforms a divergent flow of electrons emitted by a source on the *n*-side into a convergent flow on the *p*-side. This results in focusing (Fig. 2A) for a symmetric junction, $\rho_h = \rho_e$ corresponding to $n = -1$. Under the latter condition, electrons injected at $(-a,0)$ in the *n*-region at the Fermi energy meet again in a symmetric spot at $(a,0)$.

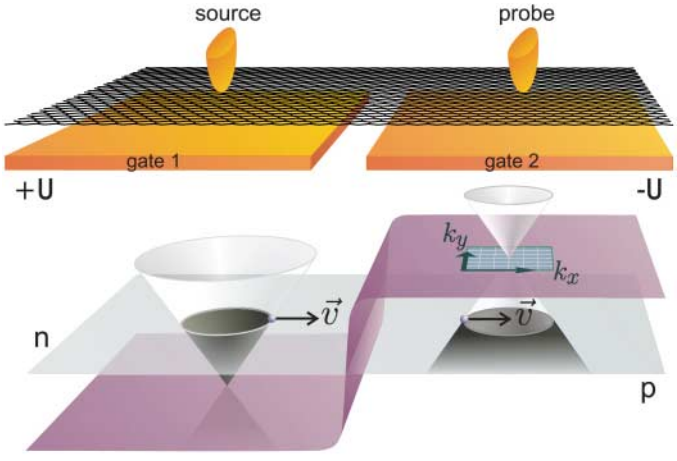

Fig. 1. Graphene *p-n* junction (PNJ). Monolayer of graphite is placed over the split gate, which is used to create *n*- (**left**) and *p*-doped (**right**) regions. The energy diagram shows the position of the Fermi level with respect to the touching point of the valence and the conduction bands.

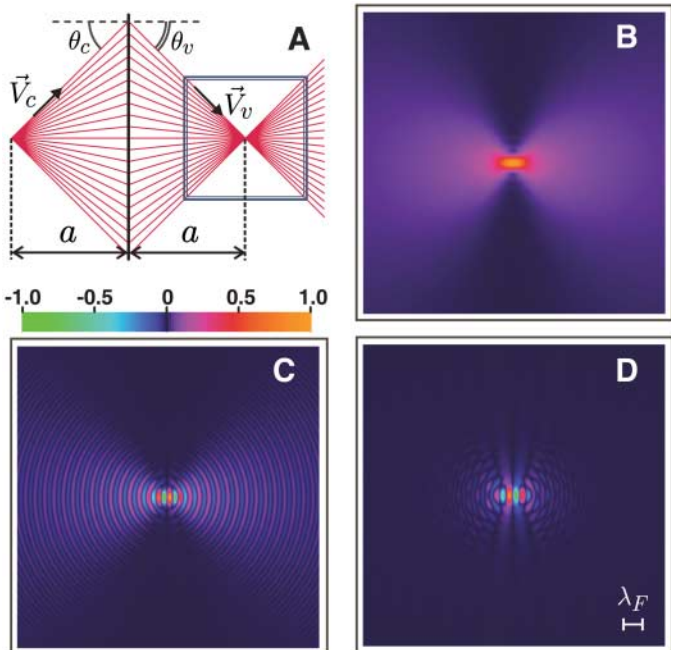

Fig. 2. Focusing of electrons by symmetric PNJ, $\rho_h = \rho_e$. (**A**) Classical trajectories of electrons diverging from a source at distance *a* from the junction become convergent after refraction. (**B**) Interference-induced pattern in the charge current near the focal image of the source-contact. (**C** and **D**) "Quantum mirage" in graphene. LDOS oscillations around the image of a perturbation applied on the other side of PNJ, created by (C) a small island of bilayer and (D) potential of a remote Coulomb charge.

[1]Physics Department, Lancaster University, Lancaster LA1 4YB, UK. [2]Physics Department, Columbia University, 538 West 120th Street, New York, NY 10027, USA. [3]NEC-Laboratories America, 4 Independence Way, Princeton, NJ 085540, USA.

*To whom correspondence should be addressed. E-mail: v.cheianov@lancaster.ac.uk

In an asymmetric junction (Fig. 3A) for, e.g., $n = -0.82$, which corresponds to $\rho_h/\rho_e = 0.67$, a sharp focus transforms into a pair of caustics that coalesce in a cusp—a singularity in the density of classical trajectories. Similar singularities in ray and wave optics were investigated and classified (*14*) with general catastrophe theory (*15*). Ballistic trajectories of electrons in the *p*-region of an asymmetric PNJ are rays $y = a\tan\theta_c + x\tan\theta_v$, where θ_v is related to θ_c by Eq. 1. The condition for a singularity, $\partial y/\partial\theta_c = 0$, determines the form of caustics $y_{caust}(x)$ as well as the position x_{cusp} of the cusp.

$$y_{caust}(x) = \pm\sqrt{\frac{\left(x^{2/3} - x_{cusp}^{2/3}\right)^3}{n^2 - 1}},\ x_{cusp} = |n|a \quad (2)$$

To detect focusing by a single flat interface in graphene, one can use a small electric contact as a source of electrons while another local probe located on the *p*-side plays the role of a detector. Electric conductance between the two contacts would reflect the probability for a carrier to get from the source to the probe. When the concentration of carriers is low, their de Broglie wavelength is big enough to envisage contacts smaller than the wavelength. To study electron transmission in a phase-coherent system between contacts of such a small size, the above-described classical picture should be complemented with the analysis of quantum interference pattern of electron de Broglie waves. Figures 2B and 3B show the result of full quantum mechanical calculations of the current of electrons emitted at $(-a,0)$ and detected by a point contact near the focal point in the symmetric PNJ (Fig. 2B) and in the vicinity of a cusp (Eq. 2) that appears when the symmetry $\rho_h = \rho_e$ is lifted off (Fig. 3B). The calculation was performed by applying the Kubo formula to the single-particle Dirac-like Hamiltonian (*2*, *7*, *8*) of electrons in graphene. It is assumed that the sample is ballistic, that is, that both the elastic and inelastic mean free path of electrons is larger than the typical size of the structure. Around, but not too close to the focus ($k_y r >> 1$), the analytically calculated current is $j \sim (x-a)^2/r^3$ [$r = \sqrt{(x-a)^2 + y^2}$ stands for the distance from the probe to the focus]. The anisotropy of the current distribution is caused by the dependence of the transmission coefficient on the incidence angle and is smeared at shorter distances $k_y r < 1$. The current map calculated in the vicinity of the cusp for $\rho_h \neq \rho_e$ shows characteristic patterns described by the canonical diffraction function for this type of wave catastrophe (*14*). The maximum of the current would be when the probe is at the tip of the cusp, $(|n|a,0)$. The width y_* of the bright spot near the cusp (Fig. 3B) or the focus (Fig. 2A) in the *y* direction can be estimated as $y_* k_y \sim \max[1,(\frac{1}{2}ak_c|n^{-1} - n|)^{1/4}]$. For a junction with $|n| > 1$ ($\rho_h > \rho_e$), the pattern near the cusp is mirror-reflected as compared with that shown in Fig. 3B for $|n| < 1$.

It has been discovered (*16*) in the scanning tunneling microscopy (STM) studies of elliptically shaped corals on the surface of copper that the presence of an impurity at one focus of the ellipse is reflected by the STM map in the vicinity of the other focus. Therefore, oscillations of the local density of states of electrons formed around a static local perturbation (*17*) can be replicated through focusing by a carefully engineered fence of atoms. Similarly, focusing of electrons by a sharp PNJ in graphene could create a "mirage" that mimics the effect of a perturbation on the opposite side of the *n-p* interface. Consider, for example, a small island of a bilayer (*5*, *18*), which locally distinguishes between two sublattices (A and B) of the honeycomb lattice for electrons in the surrounding sheet [due to Bernal stacking of two adjacent monolayers (*19*, *20*)]. It induces a change in the local electron density of states (LDOS), which is different on sublattices A and B. The long-range oscillations of the alternating LDOS can be detected, with STM, as a difference of $\delta j_{A\text{-}B} \sim j^{(0)}_{A\text{-}B}\sin(2kr)/r$ between the tunneling current from the STM tip to the A and B sites. Figure 2C shows the results (obtained with the Green's

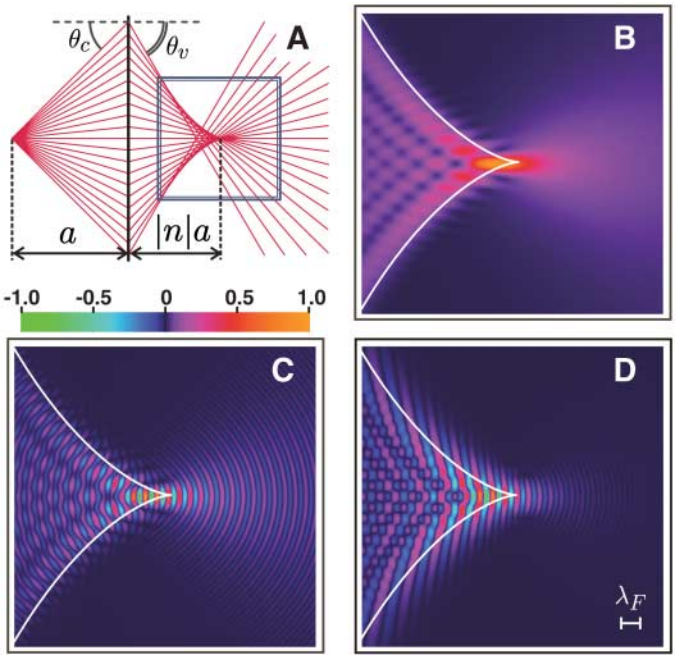

Fig. 3. Wave singularities in an asymmetric PNJ, $\rho_h/\rho_e = 0.67$. (**A**) Formation of caustics by refracted waves. (**B**) Characteristic interference pattern for the current near the cusp. (**C** and **D**) LDOS oscillations (in the region between caustics) created by (C) a small island of bilayer and (D) a remote Coulomb charge on the other side of PNJ.

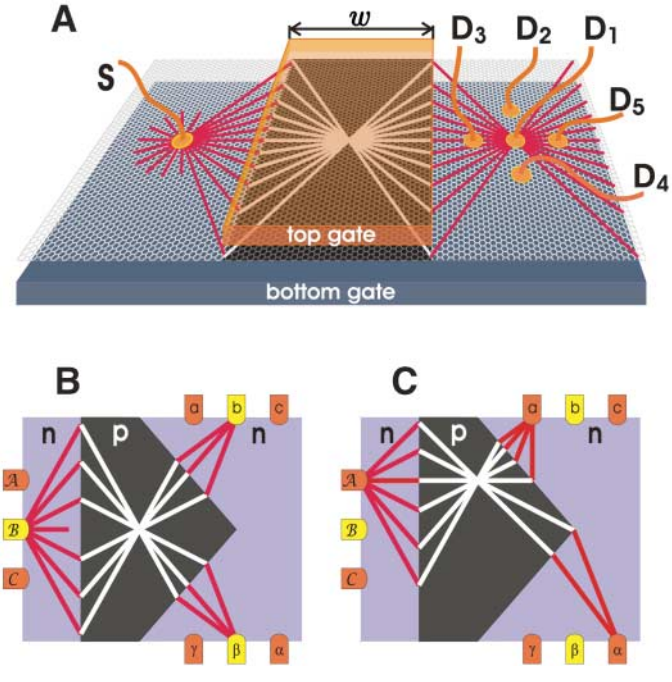

Fig. 4. (**A**) Electron Veselago lens and (**B** and **C**) prism-shaped focusing beam splitter in the ballistic *n-p-n* junction in graphene-based transistor.

functions technique) of a quantum-mechanical analysis of oscillations of $\delta j_{A\text{-}B}$ around the mirage image of a bilayer island formed on the other side of symmetric PNJ in the monolayer sheet. To compare Fig. 2D shows the calculated mirage image of a spike of electrostatic potential (smooth at the scale of the lattice constant in graphene), which induces LDOS oscillations equal on the two sublattices. The difference between these two images is caused by the lack of backscattering off A-B symmetric scatterers specific to graphene (*21*).

Unlike the ideal left-handed metamaterial (*10*), focusing in the PNJ is not perfect. In symmetric junctions, it occurs only for electrons exactly at the Fermi level, and it is spread into caustics for electrons excited to higher energies. Therefore, the sharpness of electron focusing decreases with temperature. If the focused electron flow is detected by a contact of size $d \gg \lambda_F$, a pronounced signal in the focus will persist up to $T \sim \hbar v\, k_c d/a$. For example, in a ballistic structure with $a \sim 1$ μm, $d \sim 0.1$ μm, and $\rho_e = \rho_p \sim 3 \times 10^{12}$ cm^{-2}, focusing may persist up to the nitrogen temperature. The interference effects shown in Figs. 2 and 3 are washed out at a much smaller temperature scale, $T \sim \hbar v/a$.

Focusing of electrons by a sharp *p-n* junction in graphene can be used to turn the *n-p-n* junction into a Veselago lens for electrons. In such a device (Fig. 4A), the density of charge carriers in the *p*-region (with width w) can be controlled by the top gate. If the densities in the *n*- and *p*-regions are equal ($\rho_h = \rho_e$), charge carriers injected into graphene from the contact *S* shown in Fig. 4A would meet again in the focus at the distance $2w$ from the source (contact D_3 in Fig. 4A). Varying the gate voltage over the *p*-region changes the ratio $n^2 = \rho_h/\rho_e$. This enables one to transform the focus into a cusp displaced by about $2(|n| - 1)w$ along the x axis and, thus, to shift the strong coupling from the pair of leads SD_3 to either SD_1 (for $\rho_h < \rho_e$) or SD_5 (for $\rho_h > \rho_e$). Fig. 4, B and C, illustrate another graphene-based device in which a prism-shaped top-gate may be used as a focusing beam splitter. For example, electrons emitted from contact *B* (Fig. 4B) are distributed between the contacts *b* and β, whereas the signal sent from contact *A* (Fig. 4C) is replicated into the pair of contacts *a* and α. Graphene has recently been brought into contact with a superconducting metal, and the Josephson proximity effect through graphene has been observed (*22*). Consequently, a beam splitter (Fig. 4, B and C) can be used to experiment with Einstein-Podolsky-Rosen (*23*) pairs of particles.

References and Notes

1. K. Novoselov *et al.*, *Science* **306**, 666 (2004).
2. R. Saito, G. Dresselhaus, M. S. Dresselhaus, *Physical Properties of Carbon Nanotubes* (Imperial College Press, London, 1998).
3. K. Novoselov *et al.*, *Nature* **438**, 197 (2005).
4. Y. Zhang, Y.-W. Tan, H. L. Stormer, P. Kim, *Nature* **438**, 201 (2005).
5. K. Novoselov *et al.*, *Nat. Phys.* **2**, 177 (2006).
6. T. Ohta, A. Bostwick, T. Seyller, K. Horn, E. Rotenberg, *Science* **313**, 951 (2006).
7. V. V. Cheianov, V. I. Fal'ko, *Phys. Rev. B* **74**, 041403 (2006).
8. M. Katsnelson, K. Novoselov, A. Geim, *Nat. Phys.* **2**, 620 (2006).
9. V. G. Veselago, *Sov. Phys. Usp.* **10**, 509 (1968).
10. J. B. Pendry, *Phys. Rev. Lett.* **85**, 3966 (2000).
11. J. B. Pendry, *Nature* **423**, 22 (2003).
12. D. R. Smith, J. B. Pendry, M. Wiltshire, *Science* **305**, 788 (2004).
13. M. S. Dresselhaus, G. Dresselhaus, *Adv. Phys.* **51**, 1 (2002).
14. M. Berry, *Adv. Phys.* **25**, 1 (1976).
15. V. I. Arnold, *Singularities of Caustics and Wave Fronts*; Mathematics and Its Applications Series, Vol. 62 (Kluwer, Dordrecht, 1990).
16. H. C. Manoharan, C. P. Lutz, D. M. Eigler, *Nature* **403**, 512 (2000).
17. J. Friedel, *Philos. Mag.* **43**, 153 (1952).
18. E. McCann, V. I. Fal'ko, *Phys. Rev. Lett.* **96**, 086805 (2006).
19. J. D. Bernal, *Proc. Phys. Soc. London A* **106**, 749 (1924).
20. S. Hembacher *et al.*, *Phys. Rev. Lett.* **94**, 056101 (2005).
21. V. V. Cheianov, V. I. Fal'ko, *Phys. Rev. Lett.* **97**, 226801 (2006).
22. H. B. Heersche, P. Jarillo-Herrero, J. B. Oostinga, L. Vandersypen, A. F. Morpurgo, http://arxiv.org/ftp/cond-mat/papers/0612/0612121.pdf.
23. A. Einstein, B. Podolsky, N. Rosen, *Phys. Rev.* **47**, 777 (1935).

24. This project started during the Max Planck Institute für Physik Komplexer Systeme workshop "Dynamics and Relaxation in Complex Quantum and Classical Systems and Nanostructures" and was funded by the Engineering and Physical Sciences Research Council, Lancaster Portfolio Partnership grant EP/C511743.

27 November 2006; accepted 31 January 2007
10.1126/science.1138020

Halwaxiids and the Early Evolution of the Lophotrochozoans

Simon Conway Morris[1]* and Jean-Bernard Caron[2]*

Halkieriids and wiwaxiids are cosmopolitan sclerite-bearing metazoans from the Lower and Middle Cambrian. Although they have similar scleritomes, their phylogenetic position is contested. A new scleritomous fossil from the Burgess Shale has the prominent anterior shell of the halkieriids but also bears wiwaxiid-like sclerites. This new fossil defines the monophyletic halwaxiids and indicates that they have a key place in early lophotrochozoan history.

Burgess Shale–type faunas house numerous taxa that are phylogenetically controversial and open to widely different interpretations. One approach is to incorporate these taxa into the stem groups of major phyla (*1*), but this often presupposes homologies of disparate structures and typically depends on an attenuated fossil record. Alternative views regard such taxa as either belonging to extant phyla (*2*, *3*) or representing extinct phyla (*4*). These differences have major evolutionary implications. For example, the assignment of taxa to either extant or extinct phyla implies that body plans arose by macroevolutionary mechanisms. This is consistent with body plans having a seemingly abrupt appearance and potentially with claims of a protracted (albeit cryptic) history (*5*). In contrast, hypotheses based on the construction of stem groups generally imply microevolutionary processes. The component taxa would be initiated in the latest Neoproterozoic, with body plans emerging by functional transitions that were connected to feeding, locomotion, and defense (*6*, *7*). This view is consistent with an explosive diversification of metazoans (*8*, *9*).

Numerous Cambrian groups have multiplated skeletons (or scleritomes) (*10*). Typically, the scleritomes of these groups occur as disarticulated fossils, notably in the small shelly assemblages. Burgess Shale–type faunas, however, yield articulated material such as the halkieriids, which are probably related to the siphogonuchitids [known only from disassociated sclerites (*10*)], and wiwaxiids. However, the wider relationships of these groups, the members of which are similar to armored slugs, are uncertain. One hypothesis interprets the halkieriids as stem-group lophotrochozoans, closely linking them to the origin of annelids and brachiopods (*11*).

The evolutionary route to the annelids was hypothesized to be via the related wiwaxiids (*12*), and the peculiar halkieriid arrangement of a prominent anterior and posterior shell presaged the bivalved brachiopods (*11*). More recently, the micrinids and tannuolinids, known only as isolated shells, have been interpreted as key intermediates (*13*) between the halkieriids and brachiopods. Alternative hypotheses have assigned the halkieriids to the crown-group mollusks (*3*), questioned the relevance of the micrinids and tannuolinids (*14*), and rejected the wiwaxiids as stem-group annelids (*15*). One substantial contribution to this debate is the identification of *Odontogriphus* and *Wiwaxia* as stem-group mollusks (*16*). Despite these conflicting hypotheses, the Cambrian fossil record, in principle, will be central to unravel-

[1]Department of Earth Sciences, University of Cambridge, Cambridge CB2 3EQ, UK. [2]Department of Natural History, Royal Ontario Museum, Toronto, M5S 2C6, Canada.

*To whom correspondence should be addressed. E-mail: sc113@esc.cam.ac.uk (S.C.M.); jcaron@rom.ca (J.B.C.)